Applied Surface Science 715 (2026) 164547

Contents lists available at ScienceDirect

Applied Surface Science

journal homepage: www.elsevier.com/locate/apsusc

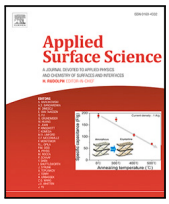

Full length article

Atomistic study of dislocation formation during Ge epitaxy on Si

Luis Martín-Encinar *, Luis A. Marqués, Iván Santos, Lourdes Pelaz

Dpto. de Electricidad y Electrónica, E.T.S.I. de Telecomunicación, Universidad de Valladolid, Paseo de Belén 15, 47011, Valladolid, Spain

ARTICLE INFO

Keywords:
Heteroepitaxial growth
SiGe
Molecular dynamics
Thin film deposition
Dislocation formation

ABSTRACT

We performed classical molecular dynamics simulations to investigate, from an atomistic point of view, the formation of dislocations during the epitaxial growth of Ge on Si. We show that simulations at 900 and 1000 K with deposition rates of 10^8 monolayers per second provide a good compromise between computational cost and accuracy. In these conditions, the ratio between the Ge deposition rate and the ad-atom jump rate is analogous to that of out-of-equilibrium experiments. In addition, the main features of the grown film (intermixing, critical film thickness, dislocation typology, and surface morphology) are well described. Our simulations reveal that dislocations originate in low-density amorphous regions that form under valleys of the rough Ge film surface. Atoms are squeezed out of these regions to the surface, releasing the stress accumulated in the film and smoothing its roughness. Amorphous regions grow until atoms begin to rearrange in dislocation half-loops that propagate throughout the Ge film. The threading arm ends of the dislocation half-loops move along the surface following valleys and avoiding islands. The film surface morphology affects the propagation path of the dislocation half-loops and the resulting dislocation network.

1. Introduction

The excellent properties of Silicon-Germanium (SiGe) and its compatibility with silicon-based technologies have promoted its use in different areas such as photonic, microelectronics, or quantum devices [1]. The heteroepitaxial growth of high-Ge-content SiGe or pure Ge layers on Si substrates entails compressive stress in the grown film due to the lattice mismatch between Si and Ge. Depending on growth conditions, the accumulated strain is elastically relaxed by generating 3D islands after the formation of a wetting layer [2], or plastically through the nucleation of misfit dislocations (MDs), threading dislocations (TDs) and partial dislocations (PDs), such as Frank PDs (FPDs) or Shockley PDs (SPDs), within the film [3].

Many experimental works have been devoted to the study of dislocations in Ge/Si systems, as they degrade the structural and electronic properties of the material. Similar detrimental effects of dislocations on device performance have also been reported in group IV, III–V, and II–VI semiconductor systems [4–6]. The main type of observed dislocations are 60° and 90° MDs, the latter being the most effective to release the strain [7]. 90° MDs have been proposed to generate through the coalescence of complementary pairs of 60° MDs [8], although some authors suggested their direct formation on the strained Ge film [9]. Dislocations originate as half-loops in the grown film [10], and their nucleation has been associated with stress concentrators related to cups and steps on the surface [11,12]. Point defects may also play a role in the formation of dislocations [13], as they do in their motion [14]. Generated dislocations can also be the source of new dislocations through multiplication mechanisms [15]. However, there is still a lack of understanding about the initial stages of dislocation nucleation at the atomic level, as experimental techniques do not allow direct observation of such processes with sufficient spatial and temporal resolution. In this context, the use of computational methods can be helpful.

Among the available computational techniques, classical molecular dynamics (CMD) allows the atomistic dynamic simulation of large enough systems to accommodate dislocations. However, because of time-scale constraints, typical experimental deposition rates cannot be directly simulated using CMD. Consequently, most CMD works on heteroepitaxial growth in the literature are either limited to very simple system cases (2D systems and elementary interatomic potentials [16]), or to simulations where dislocations are introduced *ad hoc* [14,17–19], or their nucleation is forced by incorporating surface steps [20–22]. Although these kinds of simulation offered significant information on dislocation propagation, interaction among them or with point defects, they did not provide detailed insights into the early stages of dislocation formation.

In this work, we used CMD to elucidate the atomistic origin of dislocations through a direct simulation of the heteroepitaxial growth process of Ge on Si(001). We previously analyzed the simulation conditions that can provide information comparable to that of experiments and

* Corresponding author.
E-mail address: luis.martin.encinar@uva.es (L. Martín-Encinar).

https://doi.org/10.1016/j.apsusc.2025.164547
Received 8 July 2025; Received in revised form 2 September 2025; Accepted 4 September 2025
Available online 12 September 2025

validated our CMD simulations by comparing different characteristics of the grown film with experimental observations.

2. Simulation details

To perform our CMD study, we used the Large-scale Atomic/Molecular Massively Parallel Simulator (LAMMPS) [23]. We employed the Open Visualization Tool (OVITO) [24] to visualize and analyze atomic simulation data, in particular to identify crystallographic structures and dislocations. We use the OVITO therminology throughout the paper (see Appendix A).

Atomic interactions were described by the Stillinger–Weber (SW) potential with the parameterizations of Balamane et al. [25] for Si and Posselt et al. [26] for Ge, with the Gilmer and Grabow mixing rules [27], as this particular combination is the best for describing surface dynamics and intermixing on the Si-Ge system [28].

In our simulation cell, the Si substrate consisted of a perfectly crystalline Zinc-Blende lattice containing 27 648 atoms, with a thickness of 12 monolayers (MLs) along the Z direction. This thickness was chosen to limit computational cost, as test simulations with substrates up to 20 MLs did not reveal significant differences in the nucleation and propagation mechanisms of dislocations. The dimensions of the substrate were $24\sqrt{2}a_T^{Si} \times 24\sqrt{2}a_T^{Si} \times 3\ a_T^{Si}$, being a_T^{Si} the equilibrium lattice constant of Si at temperature T and applied stress zero. The cell axes X, Y and Z were oriented along the directions [110], [−110], and [001], respectively. The upper layer atoms were arranged along Y to form the typical 2 × 1 Si(001) surface reconstruction. Periodic boundary conditions were introduced along the X and Y directions, while free boundary conditions were applied in the Z direction.

The Si substrate was divided into three zones: fixed layers, thermal bath, and surface region. The four atomic layers at the bottom were fixed to mimic bulk behavior and prevent the system from moving as a whole, as well as any spurious bending. Atoms in the four middle layers were used to create a thermal bath to control the system temperature. Atoms in the surface region and thermal bath were free to move according to Newton's dynamics. Initially, atoms in the thermal bath were given random velocities in a Maxwell–Boltzmann distribution corresponding to the desired simulation temperature, and then the whole system was equilibrated for 10^5 steps before initiating Ge deposition. The integration time step was set to 2 fs.

Ge atoms were deposited from a height of 85 Å above the substrate surface on a random (X, Y) position. Each Ge atom had an initial velocity of −0.7 nm/ps in the Z direction, corresponding to an energy of 0.185 eV (low enough to prevent substrate damage or interdiffusion into the Si substrate). We simulated the deposition of a total of 40 Ge MLs (92 160 atoms) at temperatures of 650, 800, 900 and 1000 K. To keep the substrate at the desired temperature, the atom velocities were scaled within the thermostat layers every 2000 steps. Once all Ge atoms were deposited, the system sample was equilibrated for 10^5 additional steps. To perform a statistical study, we performed five different simulations for each temperature by changing the random number seed used to select the surface impact point of the Ge atom and to generate the initial Maxwell–Boltzmann velocity distribution.

Typical deposition rates in real epitaxial growth processes range between 0.001 and 10 MLs/s [29,30], depending on the desired properties of the film. However, CMD can only reach simulation times on the order of microseconds at most, which implies that the slowest deposition rate affordable in the simulations is around 10^6 MLs/s. With this premise, CMD seems unable to simulate epitaxial Ge growth on Si under experimental conditions.

The two main factors that control film growth are the Ge deposition rate r_{dep} and the atomic surface diffusivity. When r_{dep} is low, each deposited Ge ad-atom can explore wide areas on the substrate surface and crystallize in the most favorable epitaxial positions (minimum-energy positions matching the underlying crystal lattice) before the arrival of the next ad-atom. If r_{dep} increases, the time between successive deposited Ge atoms decreases, ad-atoms move short distances on the Si surface, and tend to crystallize in kinetically trapped structures. This limitation can be compensated for increasing the temperature, which exponentially enhances diffusivity, and thus the Ge ad-atom can explore more epitaxial positions before the arrival of the subsequent Ge atom. Consequently, to compare experimental and CMD conditions, the relevant figure is the ratio between the deposition rate r_{dep} and the jump rate of ad-atoms, $\nu_d(T)$.

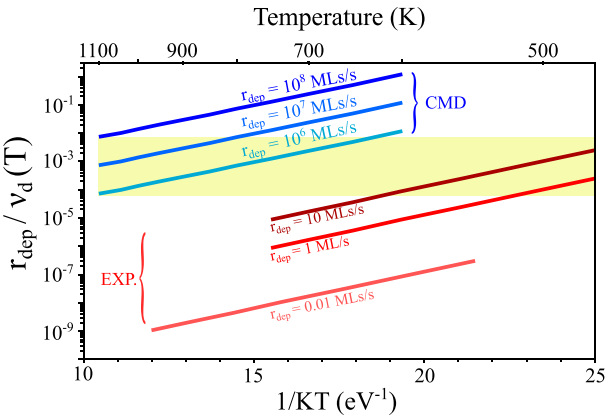

Fig. 1. Comparative of the ratio between deposition rate r_{dep} and jump rate of ad-atoms $\nu_d(T)$ for typical conditions of CMD simulations (blue lines) and experiments (red lines). The yellow band highlights ratios where CMD simulations and experimental conditions are comparable.

In Fig. 1, we plot the ratio between r_{dep} and $\nu_d(T)$ for the typical CMD and experimental growth conditions of Ge on Si. For CMD, we consider $\nu_d(T)$ calculated in Ref. [28], and deposition rates of 10^6, 10^7 and 10^8 MLs/s. For experimental conditions, we take the values for $\nu_d(T)$ extracted from Ref. [31], and consider deposition rates of 0.01, 1 and 10 MLs/s. Typically, equilibrium conditions involve low deposition fluxes (e.g. 0.001–0.1 MLs/s) and high temperatures (∼900 K), leading to the formation of 3D islands [32,33]. In contrast, out-of-equilibrium conditions are characterized by high deposition fluxes (between 0.1 and 10 MLs/s) and relatively low temperatures (around 400–500 K), leading to the formation of smooth Ge films with dislocations [34,35].

According to Fig. 1, typical experimental conditions of 3D islanding are not achievable with CMD simulations. However, with CMD at r_{dep} of 10^6 MLs/s at temperatures between 700 and 1100 K, or at 10^7 MLs/s between 900 and 1100 K, the conditions are comparable to those of experiments that lead to the formation of smooth Ge films with dislocations around 500–600 K. The deposition rate of 10^8 MLs/s is close to the limit of the CMD simulation conditions comparable to those of experiments, but it is computationally more affordable for large systems.

To verify the validity of the use of such a high r_{dep} value, we performed two test cases. First, we made sure that even the fastest r_{dep} did not induce unrealistic high-energy configurations, pronounced islands, or stacking faults (SFs) in a non-strained Ge homosystem. For that, we simulated the deposition of 54 Ge MLs on Ge(001) 2 × 1 at r_{dep} values of 10^6, 10^7 and 10^8 MLs/s, and at a temperature of 1000 K. In all simulations, we obtained Ge layers that were coherently grown on the Ge substrate according to the Frank–van der Merwe growth mode. Second, we simulated the deposition of Ge on Si(001) 2 × 1 using r_{dep} of 10^8 MLs/s and compared the results with those at a lower r_{dep} of 10^7 MLs/s, at 900 and 1000 K. We did not find significant differences in dislocation formation, their density, and origin, but the calculation times are ten times longer for the slower rate [36]. Consequently, we will use $r_{dep} = 10^8$ MLs/s in our study, as it offers a good compromise between accuracy and computational cost. In any case, the validity of the CMD simulations will be determined by comparing them with experiments whenever possible.

Table 1
Summary of the formed dislocations once deposition was completed at 650, 800, 900 and 1000 K. For simplicity, we denote dislocations using abbreviations: TD (threading dislocation), MD (misfit dislocation), FPD (Frank partial dislocation), SPD (Shockley partial dislocation), and ND (no dislocations or extended defects). The symbol ⊥ denotes orthogonal dislocations. In parenthesis, we indicate the number of formed dislocations, when there are more than one.

	650 K	800 K	900 K	1000 K
Simulation 1	Dislocation half-loop	Dislocation half-loop SPD (x2)	Two ⊥ SPDs Dislocation half-loop	Two ⊥ 90° MDs
Simulation 2	Dislocation half-loop	60° MD	90° MD	90° MD
Simulation 3	Dislocation half-loop	Dislocation half-loops (x2)	Complex dislocation network (60° and 90° MDs); FPD; SPD	Two ⊥ 90° MDs
Simulation 4	SPDs (x2)	FPD Dislocation half-loop	Complex dislocation network (60° andl 90° MDs)	SPDs (x2) (Stair rod dislocation)
Simulation 5	ND	ND	Complex dislocation network (60° and 90° MDs)	60° MD with TD 90° MD; SPD

3. Characterization of the Ge grown film

During the initial stages of Ge deposition on Si(001), we found that some Ge atoms randomly replaced Si atoms that were incorporated within the first deposited Ge layers, leading to Ge-Si intermixing. In conditions where no dislocations had yet formed, the Ge content in the original surface layer of the Si substrate ranged from 13 to 25%, according to experimental observations [37], DFT calculations [38], and kMC simulations [39], which give Ge-Si intermixing values from 10 to 20%. We noticed that intermixing increased with temperature because the atomic mobility is enhanced and the ratio between surface diffusion and intermixing frequencies decreases [28]. When dislocations nucleated and propagated down to the Si/Ge interface, severe atomic rearrangement was produced. In these cases, we found 35% Ge atoms in the original surface layer of the Si substrate, and ~10% and ~5% in the following two layers below. This observation agrees with experiments, where a higher Ge content was found in layers below the Si surface when formed dislocations reach the Si/Ge interface [40]. For further details on Ge-Si intermixing, see Supplementary Material Section S1.

The initially grown Ge layers were almost flat and "coherent" with the underlying Si substrate, until a critical thickness of the Ge film was reached and defective regions and dislocations formed. For each temperature, the critical film thickness varied widely from simulation to simulation, with a tendency to decrease as the temperature increased (see Supplementary Material Section S2). In our CMD simulations at 1000 K, we obtained critical thickness values between 10 and 20 Å, in agreement with theoretical models [41,42] and experiments [43,44].

Table 1 collects the variety of dislocations formed after 40 Ge MLs were deposited, and illustrates the stochastic nature of dislocation nucleation. Fig. 2 shows side snapshots taken during growth for representative simulation cases of each temperature. Although there is a variety of situations, we recognize some general trends. At low temperatures, the dislocations were in early growth stages or even did not form at all, due to the slow dynamics. At higher temperatures, denser dislocation networks formed, composed of TDs, 60° MDs or 90° MDs, in agreement with experimental findings [40]. This behavior is consistent with dislocation formation being a thermally activated process [45]. We also observed the formation of PDs, characterized by the presence of SFs that adopted a hexagonal diamond structure and tended to cover larger areas as the temperature increased. In some cases, the threading arms of single MDs were annihilated because of boundary conditions. The reduction of the stress in the deposited Ge film is related to the amount, type, and arrangement of the dislocation network formed (details in Supplementary Material Section S3).

In our CMD simulations, we noticed several ways to generate 90° MDs. In most cases, 90° MDs formed directly without the prior presence of 60° MDs. Sometimes (e.g. simulations 4 or 5 at 900 K), 60° MDs are combined with 90° MDs. In other cases, more frequently at higher temperatures, 90° MDs are associated with the generation of SPDs. These formation mechanisms resemble those proposed by other authors [8,9,17], although they are not as clean and ideal, since they show great complexity and variability among different simulation runs.

The surface morphology was affected by temperature and dislocation formation as Ge deposition proceeded. The roughness of the surface film was calculated as follows:

$$Roughness = \sqrt{\frac{\sum_{i=0}^{n}\left(Z_i - \overline{Z}\right)^2}{n}} \quad (1)$$

where Zi is the Z coordinate of the ith surface atom, $\overline{Z}$ is the average height of all surface atoms, and n is the total amount of surface atoms. Fig. 3 shows, for the simulations of Fig. 2, the evolution of the roughness as the deposition proceeded at different temperatures and top views of the samples after depositing 40 Ge MLs. Larger and higher 3D islands formed on the surface at lower temperatures, while the surfaces were smoother for higher temperatures. This is consistent with the enhanced surface diffusivity at higher temperatures, which favors the movement of atoms on the surface to fill denuded zones among islands, and with the increased formation of dislocations, which relax the film strain. The influence of dislocations on surface roughness is clearly evidenced, for example, in the simulation at 900 K. When a dislocation formed (after 20 Ge MLs deposited), the surface roughness decreased. As deposition progressed, the surface roughness increased and dropped again when a new dislocation nucleated (after 35 Ge MLs deposited). This cyclic behavior is consistent with experimental observations [46,47].

We have shown that CMD simulations of Ge deposition on Si, with $r_{dep} = 10^8$ MLs/s at the high-temperature range (900–1000 K), are capable of reproducing the dislocation typology and the main features of the grown film (intermixing, critical thickness, and surface roughness), in agreement with experiments under out-of-equilibrium growth conditions.

4. Atomistic insight into the origin of dislocations

From the inspection of our CMD simulations, we perceived the significant role of surface roughness in the nucleation of dislocations, as highlighted by Tersoff and LeGoues [12]. We found that the dislocations nucleated in the surface zones between islands, commonly known as valleys or depressions that act as stress concentrators. However, the specific depression site on the surface where the dislocations nucleated was, in principle, unpredictable. In all our simulations, the region under the depression where the dislocations originate is characterized by local structural disorder, since OVITO identified most of their atoms as *other* (see Appendix A). Consequently, we will refer to these zones that preceded dislocations as *disordered regions*.

Considering the roughness and the large amount of micro-islands and valleys on the surface, there was a high density of sites where dislocations could initially nucleate. In fact, we noticed that small disordered regions often appeared simultaneously in different valleys. During deposition, one of these regions, usually located in the most

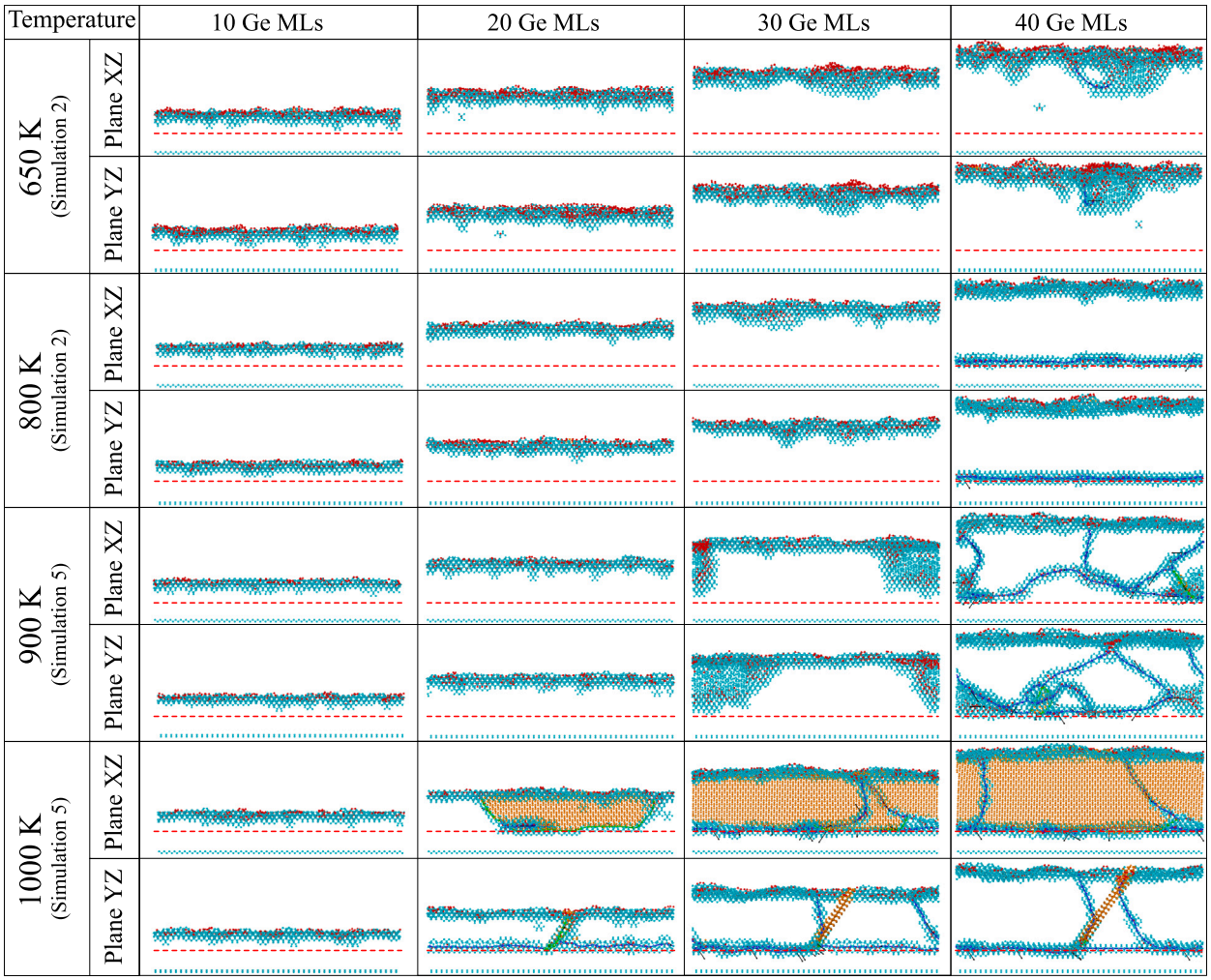

Fig. 2. Side views of samples during the Ge epitaxial growth process at different temperatures. The corresponding simulated case of Table 1 is indicated in parenthesis. Only non-cubic diamond atoms are shown. Atoms are colored according to their local structure: cubic diamond up to 1st or 2nd neighbors (■), hexagonal diamond (■), and *other* (■). Dark blue and green lines indicate dislocations with (a/2) <110> and (a/6) <112> Burgers vectors (black arrows), respectively. Horizontal red dashed lines indicate the original position of the Si surface substrate.

extensive valley, evolved to a deeper and larger disordered region with the shape of a half-loop along a specific crystallographic plane (mostly (100), (001) or {011}). During the growth of the disordered region, we found that some of the Ge atoms inside moved towards the surface, thus generating "vacancies" within that region. This contributed to strain relaxation and prevented the evolution of other incipient disordered regions on the surface.

In all of our simulations, we found that valleys in the rough surface Ge film also played a significant role in the propagation of dislocations. The ends of the threading arms of the dislocation half-loops, which were also formed by disordered atoms, moved along the surface through the valleys avoiding islands, thus facilitating the ejection of more Ge atoms from the film. The presence of islands in the propagation pathway of dislocations forced them to change their expansion direction or even to split, leading to dislocation multiplication. Thus, specific surface morphology affects the resulting dislocation network (see Supplementary Material Section S4).

In order to illustrate the process of dislocation formation, in Fig. 4 we show several snapshots taken during one of the Ge deposition simulations carried out at 900 K (simulation 2 of Table 1). At $t = 400$ ns, ≈35 MLs deposited, islands (red regions in the upper panels) with a height of around 1.5 nm with respect to valleys (dark blue regions in the upper panels) were formed, and an incipient disordered region (red atoms in the middle and bottom panels) was generated in one of the valleys. At $t = 410$ ns, ≈35.5 MLs deposited, the disordered region increased its size along the crystallographic plane (100), aligned with the valley in which it lay. At $t = 415$ ns, ≈36 MLs deposited, the disordered zone rearranged with the shape of a half-loop lying on a plane {111}. Later, the threading arms of the half-loop moved along the surface through the valleys, avoiding islands, which produced kinks in the generated 90° MD line. Eventually, both dislocation threading arms met due to periodic boundary conditions at $t = 450$ ns, ≈39 MLs deposited. Under additional annealing, this line defect transformed into a perfectly straight 90° MD (see Supplementary Material Section S5).

To study the evolution of stress in the Ge film during the process of dislocation formation, we have evaluated the atomic stress tensor, which is calculated for a given atom i with the virial expression:

$$S_i^{ab} = -\frac{1}{V_i}\sum_{j\neq i}(m_i v_i^a v_i^b + F_{ij}^a |r_{ij}^b|), \quad (2)$$

where a and b take the values x, y or z. m_i and v_i are the atomic mass and velocity of the atom i, respectively. F_{ij} is the interatomic force applied to the particle i by particle j. r_{ij} is the vector between particles i and j. V_i is the atomic volume, which is computed using the *Voronoi volume*. Since the Voronoi volume cannot be calculated for atoms lying on a surface, we assumed for simplicity that for film surface atoms V_i is equal to the Voronoi volume of an atom in a perfect diamond lattice site.

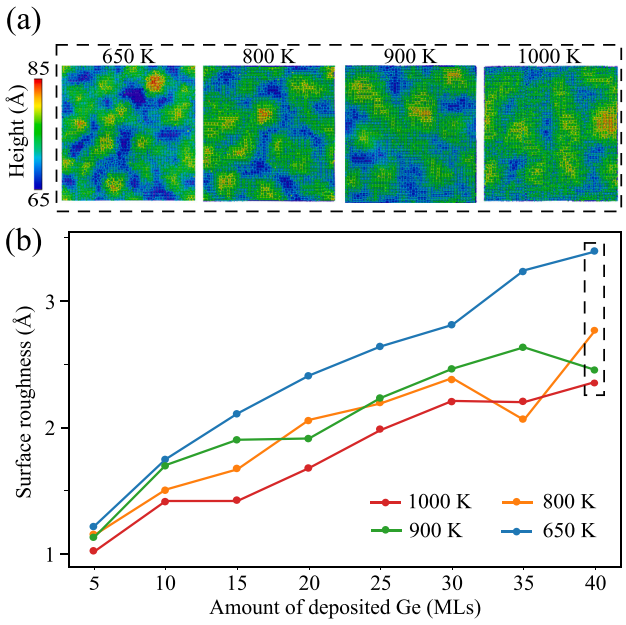

Fig. 3. (a) Top views of the samples corresponding to the simulations in Fig. 2 after depositing 40 Ge MLs. Atoms are colored according to their height. (b) Surface roughness as a function of the number of deposited Ge MLs at different temperatures for the simulation cases of Fig. 2.

Fig. 5 shows the evolution of S_i^{xx} for atoms within a 17 Å slice in a (100) plane around the disordered region that was generated during the Ge deposition simulation at 900 K previously described. The sequence times are the same as those of the snapshots shown in Fig. 4. We focus here on the xx component of the atomic stress tensor because the final 90° MD formed along the simulation cell Y axis (S_i^{yy} and S_i^{zz} are shown in Supplementary Material Section S6). At t = 400 ns, the Ge film was under compressive stress, except for the atoms that lay on the surface. The atoms below the disordered region where the dislocation formed were under compressive stress slightly higher than that of the rest of the atoms in the Ge film, which suggests a relation between the local concentration of stress in the surface valleys and the generation of disordered regions. The release of stress within the Ge film started with the growth of the disordered region, t = 410 ns, due to the movement of some of its atoms towards the surface (vacancy generation). The formation of the dislocation half-loop at t = 415 ns and its subsequent propagation up to t = 425 ns produced a further release of stress along the Ge film. The final 90° MD, at t = 450 ns, concentrated the compressive stress of the Ge film below its core up to the Si substrate, while the Ge atoms above were relaxed, in agreement with previous observations by other authors [14].

Fig. 6 shows the evolution of the number of disordered atoms (identified as *other* atoms in OVITO) and "vacancies" (missing atoms with respect to the perfect lattice), which have been accounted for within a parallelepiped region that encompasses the dislocation in the previously described simulation (dashed rectangle in Fig. 4 indicates its top surface, its volume goes from the film surface down to the Si/Ge interface). Three different stages are distinguished:

- Stage I corresponds to the generation and growth of the initial disordered region below the surface valley of the Ge film. The initial number of disordered atoms correlates with the amount of *other* atoms which are always present on the film surface. Along with the increase in the number of disordered atoms, there is also a sharp increase in the number of vacancies within the region, which is a natural mechanism that helps to accommodate mismatch and release strain energy [48–50]. These missing atoms were squeezed out from the disordered region, moved upward, and refilled the valley, thus smoothing the surface.
- Stage II corresponds to the formation and propagation of the dislocation half-loop. Atoms in the core of the disordered region rearranged according to lattice sites, resulting in a reduction in the number of disordered atoms. The threading arms of the dislocation half-loop still contained a large number of disordered atoms. As the half-loop expanded sideways, more Ge atoms from the film moved towards the surface through the threading arms, further releasing strain. This caused an additional increase in the number of vacancies in the region, although at a slightly slower pace compared to stage I.
- Stage III corresponds to the situation where the final 90° MD dislocation was already formed. The number of disordered atoms restores to the typical value of the film surface within the region, and the final number of vacancies correlates to the number of atoms of the missing plane above the dislocation.

Given the relevance of disordered regions in the origin and propagation of dislocations, we characterized their nature. In particular, we calculated the coordination number and the radial distribution function, $g(r)$, of the atoms in the disordered region after depositing 36 Ge MLs at 900 K (the same sample shown in Fig. 4 at t = 415 ns, corresponding to the maximum size of the disordered region).

The coordination number (CN) of a given atom is defined as the number of nearest-neighbor atoms surrounding it. In our simulations, we defined nearest neighbors as atoms separated by a distance of less than 3.1 Å. This choice was based on the distance where $g(r)$ approaches zero beyond its first peak (i.e. the distance at which nearest neighbors are commonly found in the perfect crystal). Fig. 7 shows atoms with a coordination number different from four, in a perspective view of the analyzed sample. The surface atoms were under-coordinated, while the atoms with CN = 5 were abundant in the disordered region, and even some atoms with CN = 6 were identified. The shape of this region with over-coordinated atoms resembles that of Fig. 4 at t = 415 ns. However, they are not identical since fewer atoms are displayed here (many atoms classified as cubic diamond up to 1st or 2nd neighbors and some of the *other* atoms have CN = 4). We found that approximately 80% of the atoms in the disordered region had CN = 4, 15% had CN = 5, and 5% had CN = 6, which is typical of the amorphous Ge phase, *a*-Ge [51,52].

Fig. 8 compares the $g(r)$ of the disordered region identified by non-cubic diamond atoms together with the $g(r)$ extracted from samples of ideal *a*-Ge at 900 K, crystal Ge (*c*-Ge) at 900 K, and liquid Ge (*l*-Ge) at 3000 K. The $g(r)$ of the disordered region is very similar to that of ideal *a*-Ge (it does not asymptotically go to one with r due to the limited volume used for its calculation), which confirms its amorphous phase nature. Therefore, the disordered structure identified prior to dislocation formation is compatible with the *a*-Ge phase.

We also quantified the atomic local density in a parallelepiped volume encompassing the disordered structure (excluding surface atoms). In a coherently grown Ge thin film on Si, this volume should contain a total of 1550 atoms, but we found that 162 atoms were missing, which corresponds to a local atomic density ~10% below that of *c*-Ge. We also analyzed the disordered regions that preceded dislocations in the rest of our simulations and found that missing atoms corresponded to local atomic densities ranging from 5% to 15% below that of *c*-Ge. Since ideal *a*-Ge has a local density only 5% lower than *c*-Ge, our results indicate that the disordered regions actually correspond to a low-density *a*-Ge phase.

5. Conclusions

We studied the heteroepitaxial growth of Ge on Si(001) 2 × 1 using CMD simulations with the SW potential, paying special attention to dislocation formation. We showed that feasible deposition rates in

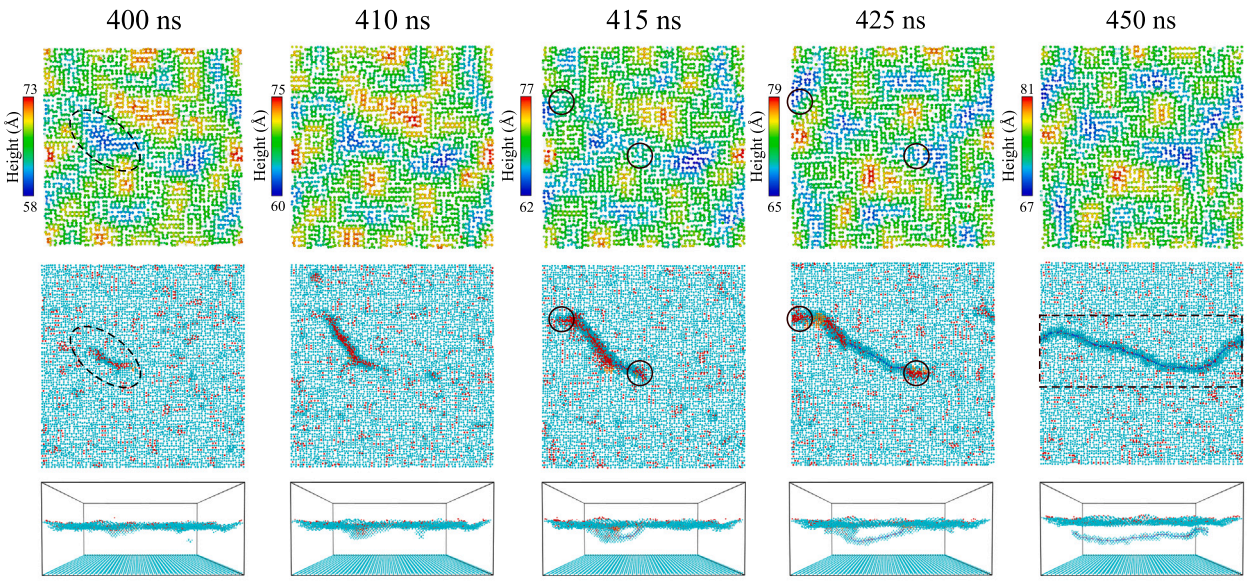

Fig. 4. Sample snapshots taken at different times during one of the deposition simulations carried at 900 K (simulation 2 of Table 1). Upper panels are top views where atoms are colored according to their height. Middle panels are also top views where atoms are colored according to their local structure: cubic diamond up to 1st or 2nd neighbors (■), hexagonal diamond (■), and *other* (■) (perfect cubic diamond atoms are not shown). Bottom panels are perspective views of atoms shown in middle panels. Dashed ovals indicate the valley and disordered region where the dislocation starts to form. Full circles highlight the position of dislocation threading arm ends. Dashed rectangle indicates the top surface of the parallelepiped region where the number of disordered atoms and vacancies are computed (shown in Fig. 6). Dark blue lines are dislocation lines as identified by OVITO.

CMD (from 10^6 to 10^8 MLs/s) at elevated temperatures (between 700 and 1100 K) allow simulation of the growth process under conditions analogous to those of experiments under out-of-equilibrium conditions (high deposition rates and low temperatures), where strain relaxation occurs through dislocation nucleation. In particular, we found that CMD simulations with deposition rates of 10^8 MLs/s and temperatures of 900 and 1000 K offer a good compromise between computational cost and accuracy. We tested that the features of the simulated grown film (critical thickness, intermixing and surface roughness) and the dislocation typology are in agreement with experiments.

We analyzed, at atomic level, the origin of dislocations and showed the interplay between surface roughness and dislocations. We observed that dislocations nucleated preferentially in valleys among islands on the surface of the Ge film, although the exact nucleation region where they appeared was, in principle, unpredictable. In all cases, regions where the dislocations nucleated had low atomic density and were of an amorphous nature. These amorphous regions grew as the deposition proceeded until they reached a critical size. The high stress in the surface valleys, along with the low density and amorphous nature of these regions, favored a local increase in atomic mobility. Some of their atoms moved towards the surface (generation of "vacancies"), thus releasing the stress accumulated in the growing Ge film. At some point, these regions recrystallized and propagated through the Ge film in the shape of a dislocation half-loop. The rough surface also played a role in the propagation of the dislocation half-loop as its ends moved along the valleys, avoiding islands on the surface, forcing the dislocation line to change directions or even splitting. In turn, the formation of dislocations modified the roughness of the surface as climbing atoms filled the valleys, and the released strain favored smoother surfaces during further deposition.

In our simulations with the SW potential at lower temperatures (650 and 800 K), even though the dislocations were in an early stage of development, we also observed the formation of amorphous regions prior to the generation of the dislocation half-loops. We also tested deposition simulations with the Tersoff potential at elevated temperatures and obtained analogous results concerning the amorphous nature of the nucleation region and its evolution (see Supplementary Material Section S7). These findings indicate that the described mechanism is not related to the specific empirical potential nor to the high temperatures used in the simulations, but it is an intrinsic feature of the early stages of dislocation formation in stressed and rough Ge films.

CRediT authorship contribution statement

Luis Martín-Encinar: Writing – original draft, Visualization, Methodology, Investigation, Formal analysis, Conceptualization. **Luis A. Marqués:** Writing – original draft, Validation, Supervision, Conceptualization. **Iván Santos:** Software. **Lourdes Pelaz:** Writing – original draft, Validation, Supervision, Project administration, Conceptualization.

Declaration of competing interest

The authors declare that they have no known competing financial interests or personal relationships that could have appeared to influence the work reported in this paper.

Acknowledgments

This work has been supported by the Spanish Ministerio de Ciencia e Innovación under Project No. PID2020-115118GB-I00.

Appendix A. Terminology used for the atomic identification of crystal structures

Following OVITO's terminology, we classify atoms in our CMD simulations as:

- Cubic diamond: atom that has all of its 1st and 2nd nearest neighbors positioned on cubic diamond lattice sites.
- Cubic diamond up to 1st neighbors: atom that is a 1st neighbor of an atom that was classified as "cubic diamond". Its four nearest neighbors are positioned on lattice sites, but at least one of its 2nd nearest neighbors is not.

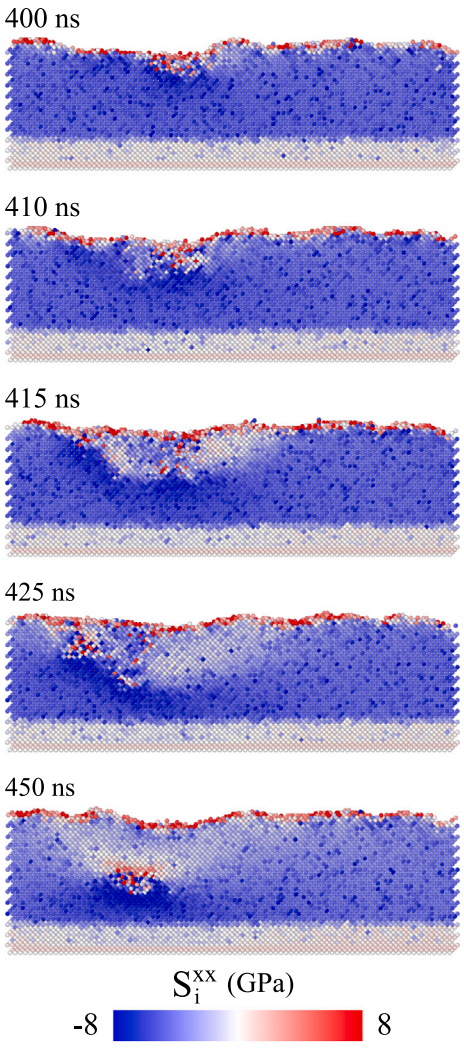

Fig. 5. Snapshots showing atoms within a 17 Å slice in a (100) plane around the disordered region whose evolution was shown in Fig. 4. Atoms are colored according to the *xx* component of the atomic stress tensor (blue means compressive and red tensile).

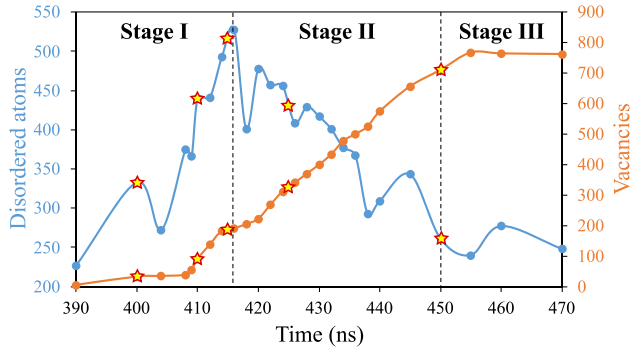

Fig. 6. Evolution of the number of *other* atoms and vacancies in a parallelepiped region encompassing the dislocation formed after deposition at 900 K (simulation 2 of Table 1). Stars indicate the times corresponding to the snapshots shown in Fig. 4.

- Cubic diamond up to 2nd neighbors: atom that is a 2nd nearest neighbor of an atom that was classified as "cubic diamond". The atom itself is positioned on a lattice site, but at least one of its neighbors is missing or is not positioned on a lattice site.
- Hexagonal diamond: here we encompass atoms that have all of its 1st and 2nd nearest neighbors positioned on hexagonal diamond lattice sites, and also those that are 1st or 2nd neighbors to them.
- *Other*: atom, with unknown coordination structure, that does not belong to any of the previous categories. This atom has a disordered local environment and is typically located inside or close to lattice defects (e.g. vacancies, interstitials, dislocations, ...), the surface or amorphous regions.

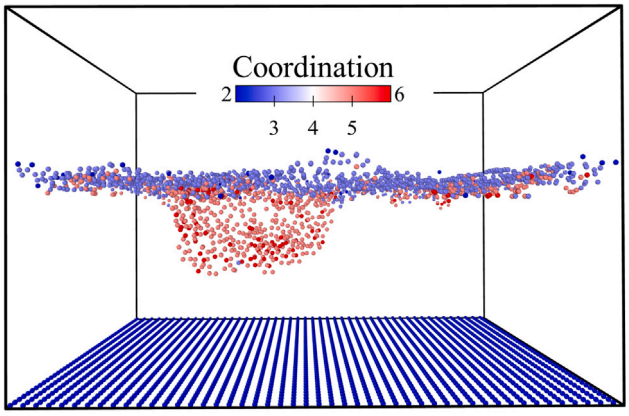

Fig. 7. Perspective view of the sample after depositing 36 Ge MLs at 900 K, where atoms are colored according to their CN. Only atoms with CN different from 4 are shown.

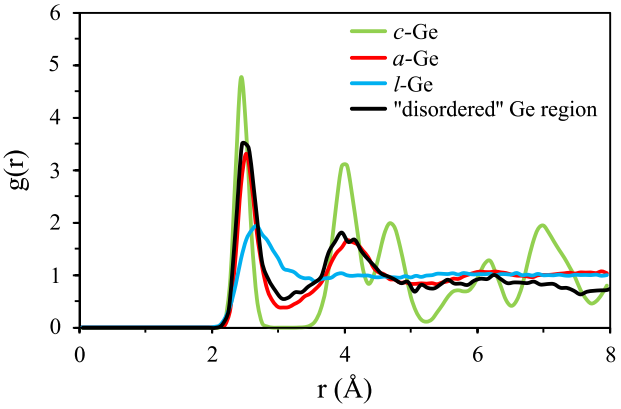

Fig. 8. Radial distribution functions of the disordered region shown in Fig. 4, and of ideal *a*-Ge (at 900 K), *c*-Ge (at 900 K) and *l*-Ge (at 3000 K) samples.

Appendix B. Supplementary data

Supplementary material related to this article can be found online at https://doi.org/10.1016/j.apsusc.2025.164547.

Data availability

Data will be made available on request.

References

[1] D. Ryzhak, J. Aberl, E. Prado-Navarrete, L. Vukušić, A.A. Corley-Wiciak, O. Skibitzki, M.H. Zoellner, M.A. Schubert, M. Virgilio, M. Brehm, G. Capellini, D. Spirito, Nanoheteroepitaxy of ge and sige on si: role of composition and capping on quantum dot photoluminescence, Nanotechnology 35 (2024) 505001, http://dx.doi.org/10.1088/1361-6528/ad7f5f.

[2] L.V. Arapkina, K.V. Chizh, V.P. Dubkov, M.S. Storozhevykh, V.A. Yuryev, Evolution of Ge wetting layers growing on smooth and rough Si(001) surfaces: Isolated 105 facets as a kinetic factor of stress relaxation, Appl. Surf. Sci. 608 (2023) 155094, http://dx.doi.org/10.1016/j.apsusc.2022.155094.

[3] Y. Du, Z. Kong, M.S. Toprak, G. Wang, Y. Miao, B. Xu, J. Yu, B. Li, H. Lin, J. Han, Y. Dong, W. Wang, H.H. Radamson, Investigation of the heteroepitaxial process optimization of Ge layers on Si (001) by RPCVD, Nanomaterials 11 (2021) http://dx.doi.org/10.3390/nano11040928.

[4] S. Zaima, O. Nakatsuka, N. Taoka, M. Kurosawa, W. Takeuchi, M. Sakashita, Growth and applications of GeSn-related group-IV semiconductor materials, Sci. Technol. Adv. Mater. 16 (2015) 043502, http://dx.doi.org/10.1088/1468-6996/16/4/043502.

[5] X. Liu, Z. Lv, Z. Liao, et al., Highly efficient AlGaN-based deep-ultraviolet light-emitting diodes: from bandgap engineering to device craft, Microsyst. Nanoeng. 10 (2024) 110, http://dx.doi.org/10.1038/s41378-024-00737-x.

[6] Katherine N. Zaunbrecher, Darius Kuciauskas, Craig H. Swartz, Pat Dippo, et al., Impact of extended defects on recombination in CdTe heterostructures grown by molecular beam epitaxy, Appl. Phys. Lett. 109 (2016) 091904, http://dx.doi.org/10.1063/1.4961989.

[7] Y. Bolkhovityanov, A. Gutakovskii, A. Deryabin, L. Sokolov, Role of edge dislocations in plastic relaxation of gesi/si(001) heteroestructures: dependence of introduction mechanisms on film thickness, Phys. Solid State 57 (2015) 765–770, http://dx.doi.org/10.1134/S1063783415040071.

[8] Y.B. Bolkhovityanov, L.V. Sokolov, Ge-on-Si films obtained by epitaxial growing: edge dislocations and their participation in plastic relaxation, Semicond. Sci. Technol. 27 (2012) 043001, http://dx.doi.org/10.1088/0268-1242/27/4/043001.

[9] T.F. Wietler, E. Bugiel, K.R. Hofmann, Relaxed germanium films on silicon (110), Thin Solid Films 517 (2008) 272–274, http://dx.doi.org/10.1016/j.tsf.2008.08.018, fifth International Conference on Silicon Epitaxy and Heterostructures (ICSI-5).

[10] Y.B. Bolkhovityanov, A.S. Deryabin, A.K. Gutakovskii, M.A. Revenko, L.V. Sokolov, Direct observations of dislocation half-loops inserted from the surface of the GeSi heteroepitaxial film, Appl. Phys. Lett. 85 (2004) 6140–6142, http://dx.doi.org/10.1063/1.1839271.

[11] D. Jesson, S. Pennycook, J.-M. Baribeau, D. Houghton, Direct imaging of surface cusp evolution during strained-layer epitaxy and implications for strain relaxation, Phys. Rev. Lett. 71 (1993) 1744–1747, http://dx.doi.org/10.1103/PhysRevLett.71.1744.

[12] J. Tersoff, F.K. LeGoues, Competing relaxation mechanisms in strained layers, Phys. Rev. Lett. 72 (1994) 3570–3573, http://dx.doi.org/10.1103/PhysRevLett.72.3570.

[13] B. Pichaud, N. Burle, M. Texier, C. Alfonso, M. Gailhanou, J. Thibault-Pénisson, C. Fontaine, V.I. Vdovin, Dislocation nucleation in heteroepitaxial semiconducting films, Phys. Status Solidi C 6 (2009) 1827–1835, http://dx.doi.org/10.1002/pssc.200881469.

[14] L. Barbisan, A. Marzegalli, F. Montalenti, Atomic-scale insights on the formation of ordered arrays of edge dislocations in Ge/Si(001) films via molecular dynamics simulations, Sci. Rep. 12 (2022) 3235, http://dx.doi.org/10.1038/s41598-022-07206-3.

[15] M. Capano, Multiplication of dislocations in $si_{1-x}ge_x$ layers on si(001), Phys. Rev. B 45 (1992) 11768–11774, http://dx.doi.org/10.1103/PhysRevB.45.11768.

[16] L. Dong, J. Schnitker, R.W. Smith, D.J. Srolovitz, Stress relaxation and misfit dislocation nucleation in the growth of misfitting films: A molecular dynamics simulation study, J. Appl. Phys. 83 (1998) 217–227, http://dx.doi.org/10.1063/1.366676.

[17] E. Maras, O. Trushin, A. Stukowski, T. Ala-Nissila, H. Jónsson, Global transition path search for dislocation formation in Ge on Si(001), Comput. Phys. Comm. 205 (2016) 13–21, http://dx.doi.org/10.1016/j.cpc.2016.04.001.

[18] E. Maras, L. Pizzagalli, T. Ala-Nissila, H. Jónsson, Atomic scale formation mechanism of edge dislocation relieving lattice strain in a GeSi overlayer on Si(001), Sci. Rep. 7 (2017) 11966, http://dx.doi.org/10.1038/s41598-017-12009-y.

[19] O. Trushin, E. Maras, A. Stukowski, E. Granato, S.C. Ying, H. Jónsson, T. Ala-Nissila, Minimum energy path for the nucleation of misfit dislocations in Ge/Si(001) heteroepitaxy, Modelling Simul. Mater. Sci. Eng. 24 (2016) 035007, http://dx.doi.org/10.1088/0965-0393/24/3/035007.

[20] X. Zhang, W. Cai, Critical strain for surface nucleation of dislocations in silicon, 2018, arXiv:1806.01974.

[21] K. Shima, S. Izumi, S. Sakai, Reaction pathway analysis for dislocation nucleation from a sharp corner in silicon: Glide set versus shuffle set, J. Appl. Phys. 108 (2010) 063504, http://dx.doi.org/10.1063/1.3486465.

[22] Z. Li, R.C. Picu, R. Muralidhar, P. Oldiges, Effect of Ge on dislocation nucleation from surface imperfections in Si-Ge, J. Appl. Phys. 112 (2012) 034315, http://dx.doi.org/10.1063/1.4745864.

[23] A.P. Thompson, H.M. Aktulga, R. Berger, D.S. Bolintineanu, W.M. Brown, P.S. Crozier, P.J. in 't Veld, A. Kohlmeyer, S.G. Moore, T.D. Nguyen, R. Shan, M.J. Stevens, J. Tranchida, C. Trott, S.J. Plimpton, LAMMPS - a flexible simulation tool for particle-based materials modeling at the atomic, meso, and continuum scales, Comp. Phys. Comm. 271 (2022) 108171, http://dx.doi.org/10.1016/j.cpc.2021.108171.

[24] A. Stukowski, Visualization and analysis of atomistic simulation data with OVITO–the Open Visualization Tool, Modelling Simul. Mater. Sci. Eng. 18 (2009) 015012, http://dx.doi.org/10.1088/0965-0393/18/1/015012.

[25] H. Balamane, T. Halicioglu, W.A. Tiller, Comparative study of silicon empirical interatomic potentials, Phys. Rev. B 46 (1992) 2250–2279, http://dx.doi.org/10.1103/PhysRevB.46.2250.

[26] M. Posselt, A. Gabriel, Atomistic simulation of amorphous germanium and its solid phase epitaxial recrystallization, Phys. Rev. B 80 (2009) 045202, http://dx.doi.org/10.1103/PhysRevB.80.045202.

[27] M.H. Grabow, G.H. Gilmer, Thin film growth modes, wetting and cluster nucleation, Surf. Sci. 194 (1988) 333–346, http://dx.doi.org/10.1016/0039-6028(88)90858-8.

[28] L. Martín-Encinar, L.A. Marqués, I. Santos, P. López, L. Pelaz, Concurrent characterization of surface diffusion and intermixing of Ge on Si: A Classical Molecular Dynamics study, Adv. Theory Simul. 6 (2023) 2200848, http://dx.doi.org/10.1002/adts.202200848.

[29] J.-O. Carlsson, P.M. Martin, Chapter 7 - Chemical vapor deposition, in: Handbook of Deposition Technologies for Films and Coatings (Third Edition), third ed., William Andrew Publishing, 2010, pp. 314–363, http://dx.doi.org/10.1016/B978-0-8155-2031-3.00007-7.

[30] P. Frigeri, L. Seravalli, G. Trevisi, S. Franchi, 3.12 - Molecular beam epitaxy: An overview, in: P. Bhattacharya, R. Fornari, H. Kamimura (Eds.), Comprehensive Semiconductor Science and Technology, Elsevier, Amsterdam, 2011, pp. 480–522, http://dx.doi.org/10.1016/B978-0-44-453153-7.00099-7.

[31] M.G. Lagally, An atomic-level view of kinetic and thermodynamic influences in the growth of thin films, Japan. J. Appl. Phys. 32 (1993) 1493–1501, http://dx.doi.org/10.1143/jjap.32.1493.

[32] N. Radić, B. Pivac, P. Dubček, I. Kovačević, S. Bernstorff, Growth of Ge islands on Si substrates, Thin Solid Films 515 (2006) 752–755, http://dx.doi.org/10.1016/j.tsf.2005.12.198.

[33] G. Capellini, M. De Seta, F. Evangelisti, Ge/Si(100) islands: Growth dynamics versus growth rate, J. Appl. Phys. 93 (2003) 291–295, http://dx.doi.org/10.1063/1.1527211.

[34] D. Choi, Y. Ge, J.S. Harris, J. Cagnon, S. Stemmer, Low surface roughness and threading dislocation density Ge growth on Si (001), J. Cryst. Growth 310 (2008) 4273–4279, http://dx.doi.org/10.1016/j.jcrysgro.2008.07.029.

[35] V. Shah, A. Dobbie, M. Myronov, D. Leadley, High quality relaxed Ge layers grown directly on a Si(001) substrate, Solid-State Electron. 62 (2011) 189–194, http://dx.doi.org/10.1016/j.sse.2011.03.005.

[36] Simulations were run using 112 CPU threads in two Intel(R) Xeon(R) Gold 6238R processors: while for $r_{dep}=10^7$ MLs/s they lasted, on average, about 45 days, with $r_{dep}=10^8$ MLs/s they lasted 5 days.

[37] A. Ikeda, K. Sumitomo, T. Nishioka, T. Yasue, T. Koshikawa, Y. Kido, Intermixing at Ge/Si(001) interfaces studied by surface energy loss of medium energy ion scattering, Surf. Sci. 385 (1997) 200–206, http://dx.doi.org/10.1016/S0039-6028(97)00275-6.

[38] J.-H. Cho, M.-H. Kang, Ge-Si intermixing at the Ge/Si(001) surface, Phys. Rev. B 61 (2000) 1688–1691, http://dx.doi.org/10.1103/PhysRevB.61.1688.

[39] R.J. Wagner, E. Gulari, Simulation of Ge/Si intermixing during heteroepitaxy, Phys. Rev. B 69 (2004) 195312, http://dx.doi.org/10.1103/PhysRevB.69.195312.

[40] R.D. Arroyo, F. Isa, G. Isella, R. Erni, H. von Känel, P. Gröning, M.D. Rossell, Effect of thermal annealing on the interface quality of Ge/Si heterostructures, Scr. Mater. 170 (2019) 52–56, http://dx.doi.org/10.1016/j.scriptamat.2019.05.025.

[41] J.W. Matthews, Defects associated with the accommodation of misfit between crystals, J. Vac. Sci. Technol. 12 (1975) 126–133, http://dx.doi.org/10.1116/1.568741.

[42] R. People, J.C. Bean, Calculation of critical layer thickness versus lattice mismatch for Ge_xSi_{1-x}/Si strained-layer heterostructures, Appl. Phys. Lett. 47 (1985) 322–324, http://dx.doi.org/10.1063/1.96206.

[43] J. Bean, L.C. Feldman, A. Fiory, S.t. Nakahara, I. Robinson, Ge_xSi_{1-x}/Si strained-layer superlattice grown by molecular beam epitaxy, J. Vac. Sci. Technol. A: Vac. Surf. Films 2 (1984) 436–440, http://dx.doi.org/10.1116/1.572361.

[44] D.C. Houghton, D.D. Perovic, J. Baribeau, G.C. Weatherly, Misfit strain relaxation in Ge_xSi_{1-x}/Si heterostructures: The structural stability of buried strained layers and strained-layer superlattices, J. Appl. Phys. 67 (1990) 1850–1862, http://dx.doi.org/10.1063/1.345613.

[45] A. Janzen, I. Dumkow, M. Horn-von Hoegen, Thermal activation of dislocation array formation, Appl. Phys. Lett. 79 (2001) 2387–2389, http://dx.doi.org/10.1063/1.1408599.

[46] F.K. LeGoues, M.C. Reuter, J. Tersoff, M. Hammar, R.M. Tromp, Cyclic growth of strain-relaxed islands, Phys. Rev. Lett. 73 (1994) 300–303, http://dx.doi.org/10.1103/PhysRevLett.73.300.

[47] F. Rovaris, R. Bergamaschini, F. Montalenti, Modeling the competition between elastic and plastic relaxation in semiconductor heteroepitaxy: From cyclic growth to flat films, Phys. Rev. B 94 (2016) 205304, http://dx.doi.org/10.1103/PhysRevB.94.205304.

[48] G. Bauer, F. Schäffler, Self-assembled Si and SiGe nanostructures: New growth concepts and structural analysis, Phys. Status Solidi (A) 203 (2006) 3496–3505, http://dx.doi.org/10.1002/pssa.200622405.

[49] V. Bulatov, W. Cai, Computer Simulations of Dislocations, in: Oxford Series on Materials Modelling, Oxford University Press, Inc., USA, 2006.
[50] M. Myronov, Chapter 3 - Molecular beam epitaxy of high mobility silicon, silicon germanium and germanium quantum well heterostructures, in: Molecular Beam Epitaxy (Second Edition), second ed., Elsevier, 2018, pp. 37–54, http://dx.doi.org/10.1016/B978-0-12-812136-8.00003-7.
[51] J.K. Bording, Molecular-dynamics simulation of Ge rapidly cooled from the molten state into the amorphous state, Phys. Rev. B 62 (2000) 7103–7109, http://dx.doi.org/10.1103/PhysRevB.62.7103.
[52] M. Lai, X. Zhang, F. Fang, Crystal orientation effect on the subsurface deformation of monocrystalline germanium in nanometric cutting, Nanoscale Res. Lett. 12 (2017) 296, http://dx.doi.org/10.1186/s11671-017-2047-3.